CRISPR-mediated Multiplexed Live Cell Imaging of Nonrepetitive Genomic Loci

Patricia A. Clow[1], Menghan Du[1,2], Nathaniel Jillette[1], Aziz Taghbalout[1], Jacqueline J. Zhu[1,5]*, Albert W. Cheng[1,2,3,4,5]*

[1]The Jackson Laboratory for Genomic Medicine, Farmington, CT 06032, USA

[2]Department of Genetics and Genome Sciences, University of Connecticut Health Center, Farmington, CT 06030, USA

[3]The Jackson Laboratory Cancer Center, Bar Harbor, ME 04609, USA

[4]Institute for Systems Genomics, University of Connecticut Health Center, Farmington, CT 06030, USA

[5]School of Biological and Health Systems Engineering, Arizona State University, Tempe, AZ 85281, USA

*Correspondence to: albert@cheng.bio or jacquelinejufenzhu@gmail.com

Abstract

Three-dimensional (3D) structures of the genome are dynamic, heterogeneous and functionally important. Live cell imaging has become the leading method for chromatin dynamics tracking. However, existing CRISPR- and TALE-based genomic labeling techniques have been hampered by laborious protocols and are ineffective in labeling non-repetitive sequences. Here, we report a versatile CRISPR/Casilio-based imaging method that allows for a nonrepetitive genomic locus to be labeled using one guide RNA. We construct Casilio dual-color probes to visualize the dynamic interactions of DNA elements in single live cells in the presence or absence of the cohesin subunit RAD21. Using a three-color palette, we track the dynamic 3D locations of multiple reference points along a chromatin loop. Casilio imaging reveals intercellular heterogeneity and interallelic asynchrony in chromatin interaction dynamics, underscoring the importance of studying genome structures in 4D.

Main

Three-dimensional (3D) organization of the genome has pervasive roles in the regulation of transcription, DNA replication, and DNA repair[1-3]. Sequencing methods[4, 5] can uncover genome-wide chromatin interactions in bulk cell populations but are unable to resolve intercellular heterogeneity or temporal dynamics (the “fourth dimension”) which instead require live cell imaging techniques[6]. Four-dimensional (4D) live cell imaging of genomic loci can be achieved by inserting into the target loci large tandem arrays of sequences that are bound by well-characterized DNA binding domains fused to fluorescent proteins providing important insights into the dynamics of chromatin interaction and transcription[7, 8]. However, these techniques require tedious genome engineering and can be confounded by the side effects of

43 disruptive introduction of exogenous sequences at the target loci. Live-cell imaging of the
44 unmodified genome can be conducted with the use of fluorescent proteins fused to
45 programmable DNA binding proteins such as zinc finger proteins (ZFPs) and transcription
46 activator-like effectors (TALEs), but the complicated cloning protocols requiring weeks of
47 development limit their scalability[9-12]. CRISPR/Cas systems offer versatile DNA binding
48 proteins (e.g., Cas9) that can be programmed by a target-specific guide RNA (gRNA),
49 revolutionizing the field of genome biology[13]. Fluorescent proteins or fluorophores recruited
50 by dCas9 or assembled on the gRNA scaffold offer easily programmable platforms for live cell
51 genomic imaging[14-20]. However, despite current techniques providing robust labeling of
52 repetitive sequences using a single gRNA, imaging of nonrepetitive sequences requires
53 simultaneous delivery of up to tens of gRNA to achieve sufficient signal, precluding broad
54 adoption.

55 We previously engineered a modular multitasking CRISPR/Cas-based platform called
56 Casilio by combining dCas9 and engineered Pumilio/FBF (PUF)-tethered effectors[21] (**Fig. 1**).
57 An effector domain carrying out a specific function (e.g., transcription activation) is fused to a
58 unique PUF RNA binding domain that can bind to one or more copies of a specific 8-mer motif
59 inserted to the 3' end of a gRNA. PUF domains contain peptide subunits that can each be
60 programmed to recognize an RNA-base by changing amino acids contacting the RNA, thereby
61 allowing designed PUF domains to bind different 8-mer sequences[22, 23]. Casilio capitalizes on
62 the versatility of PUF domains to allow simultaneous and orthogonal delivery of effector
63 functions to distinct genome loci, as well as multimerization of effector molecules, for efficient
64 epigenetic editing[21, 24].

65 In this study, we developed Casilio for imaging nonrepetitive DNA sequences. We
66 reasoned that the immense multimerization capability of Casilio will enable concentration of
67 fluorescent proteins at a target locus to achieve sufficient signal using reduced number of target
68 DNA binding sites while the multiplexing capability will allow simultaneous multicolor labeling
69 of distinct loci in the same cell. We first tested Casilio for imaging nonrepetitive sequences
70 within the *MUC4* gene on chromosome 3 which was previously labeled by dCas9-EGFP direct
71 fusion with >30 gRNAs tiled over the region[14]. We designed gMUC4 which binds a
72 nonrepetitive sequence within *MUC4* and inserted 15 copies of Pumilio Binding Site c
73 (15xPBSc) to recruit Clover-PUFc. To allow the assessment of the specificity of Casilio, we co-
74 labeled the *MUC4* region with a Cy5-MUC4 DNA fluorescence *in situ* hybridization (FISH)
75 probe in U2OS and ARPE-19 cells labelled with Casilio/gMUC4 (**Fig. 2a-c**). Casilio achieves
76 highly specific labeling of the nonrepetitive locus using only one gRNA with 96% and 100%
77 specificity in U2OS and ARPE-19 cells, respectively. Additional support for specificity is that
78 the formation of fluorescent spots is dependent on the presence of dCas9 (**Fig. 2d**), and that the
79 number of fluorescent spots is consistent with the ploidy of the diploid ARPE-19 (**Fig. 2d**) and
80 haploid HAP1 (**Fig. 2e**) cells. Spot formation efficiency was around ~68% for ARPE-19 (**Fig.
81 2d**) and ~54% for HAP1 (**Fig. 2e**). These together demonstrate that robust and specific labeling
82 of nonrepetitive DNA sequence by Casilio requires only one gRNA.
83 To test whether Casilio can be applied to study the dynamics of chromatin interactions in
84 live cells, we selected a chromatin interaction, the *MASP1-BCL6*, with 362 kb genomic distance
85 between the interaction anchors from a published RAD21 ChIA-PET experiment performed in
86 ARPE-19 cells (ENCSR110JOO, Michael Snyder lab). We then designed a pair of gRNAs to
87 bind nonrepetitive sequences next to the anchors (**Fig. 3a**). We used Clover-PUFc to label the 5'

88 anchor (locus A) and PUF9R-iRFP670 to label the 3' anchor (locus B). Live cell microscopy of
89 ARPE-19 cells transfected with dual-color Casilio probe pairs revealed dynamic chromatin
90 interactions at second timescales and showcased a high degree of intercellular heterogeneity and
91 interallelic asynchrony of chromatin interaction at this loop (**Fig. 3b,c; Supplementary Video 1;**
92 **Supplementary Fig. 1,2a**). Such insights cannot be readily obtained via bulk cell sequencing
93 technologies, supporting the advantages of Casilio live-cell imaging for studying the dynamics of
94 chromatin interactions at single cell and single allele level. To provide future users a method to
95 assess the specificity of labeling in live-cell settings, we developed a "competitor" assay. Here, a
96 "cold" specific competitor gRNA without any PBS sites for fluorescent protein recruitment, but
97 overlaps the target, is co-introduced into cells to interfere with the binding of Casilio imaging
98 complexes and the formation of target spots (**Fig. 3d**). A non-specific competitor gRNA that
99 does not overlap the target (such as GAL4[25]) is used as a control. To denote a competitor
100 gRNA, we prefix the target with "c" to mean cold or competitor. Specific competitor gRNA cA
101 overlapping with *MASP1-BCL6* locus A greatly reduced the formation of the Clover spots
102 compared to non-specific competitor cGAL4 control (**Fig. 3e**). As expected, the iRFP670 spots
103 formed at the non-interfered location (*MASP1-BCL6* locus B) served as an internal control that
104 was unaffected by either competitor gRNAs.
105 To test if Casilio can be applied to study the function of cohesin complexes in chromatin
106 interactions, we took advantage of an engineered HCT116 cell line with endogenous RAD21
107 fused to an auxin-inducible degron (AID)[26] that allows for the conditional depletion of RAD21
108 by auxin treatment. A previous study performed Hi-C assays on this cell line and demonstrated
109 that the depletion of RAD21 in HCT116 cells resulted in loss of loop domains including a ~500
110 kb loop domain between the *IER5L* promoter (IER5L-P) and its super-enhancer (IER5L-SE)[27].

111 We used Clover-PUFc and PUF9R-iRFP670 to label the *IER5L* promoter and super-enhancer,
112 respectively (**Fig. 4a; Supplementary Fig. 3**), and performed live-cell microscopy on untreated
113 (-Auxin) (**Fig. 4b; Supplementary Video 2; Supplementary Fig. 2b,4**) and RAD21-depleted
114 (+Auxin) cells (**Fig. 4c; Supplementary Video 3; Supplementary Fig. 2c,5**). Depletion of
115 RAD21 led to farther pairwise distances of the Casilio spots in cells treated with auxin compared
116 to the untreated control, with medians of 2.09 μm and 1.21 μm, respectively (Mann-Whitney
117 two-sided p-value<0.00001) (**Fig. 4d**), consistent with the reduced interaction between the
118 promoter and super enhancer of *IER5L* upon RAD21 depletion[27]. We also used Casilio to
119 image a "RAD21-independent" interaction that displayed an opposite behavior[27], in which
120 interaction frequency increased upon RAD21 depletion (**Fig. 4e**). Consistent with the
121 observation obtained by sequencing experiments, pairwise distances of Casilio spots decreased
122 upon auxin-mediated RAD21-depletion, with medians of 1.24 μm and 0.57 μm, respectively
123 (Mann-Whitney two-sided p-value<0.00001), for the untreated and auxin-treated cells (**Fig 4f-h;**
124 **Supplementary Videos 4,5; Supplementary Fig. 2d,e**).
125 These data demonstrate that Casilio can image interaction between cis-regulatory
126 elements to study the contribution of protein factors, such as cohesin, on dynamic chromatin
127 interactions underlying gene regulation.
128 Imaging specific interactions of non-coding elements such as enhancers and promoters
129 provide new insights into gene regulation, while visualizing a continuous stretch of genomic
130 region will improve our understanding of structural folding dynamics and illuminate the process
131 of chromatin loop formation. Given that Casilio can image each nonrepetitive locus with a single
132 gRNA, we next explored the possibility of simultaneously imaging multiple nonrepetitive loci,
133 with the ultimate goal of tracking the "live" structure of a continuous genomic region. We call

134 this technique, where sequential Casilio probes are deployed across a stretch of genomic DNA,
135 "Programmable Imaging of Structure with Casilio Emitted sequence of Signal" or PISCES.
136 To increase the number of nonrepetitive loci that can be labelled, we developed a three-
137 color palette. We used three gRNAs (IER5L P-20xPBS_{48107}, M-20xPBSc, and SE-25xPBS9R)
138 (**Fig. 5a**) for labeling three nonrepetitive locations at the *IER5L* P-SE loop, with a three-color
139 fluorescent protein palette consisting of Clover-PUF_{48107}, iRFP670-PUFc, and PUF9R-mRuby2
140 (**Fig. 5b,c; Supplementary Videos 6,7; Supplementary Fig. 2f,g,6**). These experiments
141 demonstrated the use of dual or triple-color fluorescent protein combinations to encode a
142 sequence of PISCES probes for visualizing multiple reference points along a genomic region.
143 In this study, we present a CRISPR/Cas-based method for live cell fluorescence imaging
144 of nonrepetitive genomic loci with low gRNA requirement (one gRNA/locus) and high
145 spatiotemporal resolutions. We applied Casilio to visualize the dynamic interactions of DNA
146 elements in native, unmodified chromosomes, in the presence or absence of RAD21, showing
147 RAD21-dependent and independent loops display opposite behaviors upon RAD21 depletion. By
148 developing a three fluorescent protein palette, we showed that chromatin loops can be imaged at
149 multiple reference points over time. These revealed the highly heterogeneous and dynamic
150 nature of chromatin interactions and structural changes not attainable with bulk cell sequencing
151 approaches, underscoring the need for studying the 4D nucleome with high spatiotemporal
152 resolution in live cells. Although gRNA-scaffold methods based on MS2 hairpin have been
153 attempted before to reduce gRNA requirement for non-repetitive DNA labeling, the addition of
154 14 or more MS2 hairpins to gRNA greatly reduce its expression[18], whereas in Casilio, addition
155 of up to 47 copies of PBS did not affect dCas9 binding activity[21]. The high signal of target-
156 bound Casilio complexes compared to the background unbound complexes can be explained by

157 the observation that gRNA is unstable unless complexed with dCas9 at the target sites[20]. These
158 unique properties of Casilio enable the reduction of its gRNA requirement compared with
159 previously published CRISPR-based approaches. Therefore, Casilio not only significantly
160 reduces the technical challenge of using live cell imaging to study chromatin interactions in hard-
161 to-transfect cells, but also it simplifies the design of genome-wide gRNA libraries for imaging.
162 One caveat to bear in mind when conducting and interpreting live-cell genome imaging
163 experiments is the potential of the interference of the natural genome folding processes by the
164 binding of the CRISPR reagents, which might be partially alleviated with careful gRNA designs.
165 It is thus an important future goal to systematically evaluate probe design and produce a design
166 pipeline that takes into account the potential interference of the underlying genome folding
167 processes under investigation. Future development of the Casilio imaging toolkit should include
168 higher-density PISCES probe-set with an expanded palette of fluorescent proteins, in order to
169 enable the folding of the genomic region to be delineated at a higher resolution. The multiplexing
170 and expandable nature of Casilio in adapting new effector functions[21], in combination with the
171 advance in genomic imaging demonstrated here, will enable "on-the-fly" and "plug-and-play"
172 perturbation of the (epi)genome (e.g., using Casilio activator, repressor and epigenetic editing
173 modules[21, 24]) and concurrent read-out of dynamic 3D chromatin interactions, thereby
174 providing unprecedented flexibility and power for the study of the 4D nucleome (**Fig. 1b**).
175
176

Methods

Design of chromatin interaction imaging experiments

Fastq files of ARPE-19 RAD21 ChIA-PET experiment (ENCSR110JOO) were downloaded from ENCODE database and processed by ChIA-PET2[28]. Interactions were ranked by PET count. Top-ranked interactions with different PET distances were selected. To avoid interference of CTCF binding, design regions were selected by shifting external to PET regions. JACKIE[29] was then used to identify unique 1-copy CRISPR sites in the hg38 genome overlapping design regions of selected loops and further filtered for specificity by Cas-OFFinder[30]. ChIA-PET loops are displayed on WashU EpiGenome Browser (https://epigenomegateway.wustl.edu/).

Cloning for Casilio imaging

The lentiviral dCas9 expression plasmid (lenti-dCas9-Blast) was generated by PCR-based mutagenesis of lentiCas9-Blast plasmid (Addgene #52962). Clover fused with PUF RNA-binding domain were previously described: pAC1447 (Clover_PUFc) (Addgene #73689). PUF9R-tethered iRFP670 and mRuby2 were created by a combination of PCR (from IDT gBlocks) and ligation cloning placing iRFP670[31] or mRuby2[32], respectively, downstream of PUF9R. PUFc-tethered iRFP670 and PUF_{48107} tethered Clover was created by a combination of PCR (from IDT gBlocks) and ligation cloning placing iRFP670[31] upstream of PUFc or Clover upstream of PUF_{48107}, respectively. These PUF-fluorescent protein fusions contain nuclear localization signal (NLS) for their localization in the nucleus.

Guide RNA are under control of the human U6 promoter. gRNA spacer sequences were cloned into sgRNA-PBS expression vectors pCR8-sgRNA-15xPBSc or pCR8-sgRNA-15xPBS9R via an oligo-annealing protocol[33].

201 All plasmids were subjected to restriction diagnostic tests and sequenced to ensure

202 correct cloning. Plasmids will be available on Addgene.

203

204 ***Target sequences for gRNAs***

205 *MUC4*: GCCGGTGACAGGAAGAGTGC

206

207 <u>RAD21 loops in ARPE-19 and HCT116 cells</u>

208 *MASP1-BCL6* loop Locus A: GGGTAAGAAGCCACTAGGGT

209 *MASP1-BCL6* loop Locus B: GCATAGCCGCATTTGAAAGC

210 *IER5L*-P: GACTCCCGCGGGTCACTCGG

211 *IER5L*-SE: GCCATGCTCCGATAAGGATA

212 *IER5L*-M: GTTTACCCCAAGGGTCGCGG

213

214 <u>RAD21-independent loop in HCT116 cells</u>

215 Clover locus: GCTTGCCGACGATGGACCCAT

216 iRFP670 locus: GAGGATCGAAACGCTGATGCG

217

218 <u>Competitor gRNA design</u>

219 cGAL4: GAACGACTAGTTAGGCGTGTA

220 c(*MASP1-BCL6*)A (*MASP1-BCL6* loop Locus A competitor, dSaCas9):

221 GTGCTCCAGGGTAAGAAGCCAC

222 c*IER5L*-P: GCTTGACTCCCGCGGGTCACT

223

224 ***Cell culture***

225 Human osteosarcoma U2OS cells (ATCC® HTB-96™) were cultivated in Dulbecco's Modified
226 Eagle's Medium (DMEM) (Sigma) with 10% fetal bovine serum (Lonza), 4% Glutamax (Gibco),
227 1% Sodium Pyruvate (Gibco) and 1% penicillin-streptomycin (Gibco). Human retinal pigment
228 epithelial ARPE-19 cells (ATCC® CRL-2302™) were cultivated in DMEM/F12 (Gibco) with
229 10% fetal bovine serum (Lonza), and 1% penicillin-streptomycin (Gibco). Human chronic
230 myeloid leukemia HAP1 cells (Horizon™ C859) were cultivated in Iscove's Modified
231 Dulbecco's Medium (IMDM) with 20% fetal bovine serum (Lonza) and 1% penicillin-
232 streptomycin (Gibco). HCT116/RAD21-mAID cells were obtained from Kanemaki Lab[26]. The
233 cells were cultured in McCoy's 5A medium (ATCC) with 10% fetal bovine serum (Lonza), 2
234 mM L-glutamine (ATCC), penicillin-streptomycin (ThermoFisher Scientific). Incubator
235 conditions were humidified 37°C and 5% CO_2. Cell lines expressing constitutive dCas9 were
236 generated by transducing cells with lentiviruses prepared from a lenti-dCas9-Blast plasmid,
237 followed by Blasticidin selection.

238

239 ***Transfection***

240 U2OS/dCas9 cells were seeded at density of 100,000 cells/compartment in a 35 mm 4-
241 compartment CELLview™ cell culture dish (Greiner Bio-One) 24 hours before transfection.
242 Cells were transfected with 550 ng of sgRNA plasmid containing 15 Pumilio Binding Sites
243 (15xPBS) and 50 ng of Clover-PUF fusion plasmid, using 1.5 µl Lipofectamine 3000
244 (Invitrogen). Media was changed at 24 hours post-transfection.

245 ARPE-19/dCas9 cells were seeded at density of 80,000 cells/compartment in 35 mm 4-
246 compartment CELLview™ cell culture dish (Greiner Bio-One) 17 hours before transfection.

247 Cells were transfected with 400 ng of each sgRNA-15xPBS plasmid, 40 ng of Clover-PUFc
248 fusion plasmid, and 40ng of PUF9R-iRFP670 fusion plasmid using 1.5 µl Lipofectamine LTX
249 (Invitrogen). For competitor experiments, 400ng of the competitor plasmid was added. Media
250 was changed at 24 hours post-transfection.

251 HAP1/dCas9 cells were seeded at density of 150,000 cells/compartment in 35 mm 4-
252 compartment CELLview™ cell culture dish (Greiner Bio-One) 30 hours before transfection.
253 Cells were transfected with 400 ng of sgRNA-15xPBS plasmid and 40 ng of Clover-PUFc fusion
254 plasmid DNA using 3.5 µl Turbofectin (OriGene). Media was changed at 24 hours post-
255 transfection.

256 HCT116/RAD21-mAID/dCas9 cells were seeded at density of 60,000 cells/compartment
257 in 35 mm 4-compartment CELLview™ cell culture dish the day before transfection. For each
258 well, cells were transfected with 300 ng of each sgRNA plasmid and 40 ng of each fluorescent
259 protein plasmid using 3.5 µL TurboFectin (OriGene). For competitor experiments, 300 ng of the
260 competitor plasmid was added. For three-color experiments, cells were transfected with 400ng of
261 each sgRNA plasmid, 40ng of Clover-PUF_{48107} fusion plasmid, 40ng of iRFP670-PUFc fusion
262 plasmid, and 400ng of PUF9R-mRuby2 fusion plasmid using 3.5 µL TurboFectin (OriGene).
263 Media was changed at 24 hours post-transfection. Degradation of the AID-tagged RAD21 was
264 induced by the addition of 500 µM (final concentration) indole-3-acetic acid (IAA/auxin; Sigma
265 Aldrich) during media change 24 hours prior to imaging if applicable.

266

267 ***Live-cell confocal microscopy***

268 Imaging was performed at 41-51 hours post-transfection. Prior to imaging, cells were stained
269 with 0.5-1.0 µg/ml Hoechst 33342 prepared in cell culture media for 15-30 minutes, followed by

270 two media washes. Images were acquired with the Dragonfly High Speed Confocal Platform 505
271 (Andor) using an iXon EMCCD camera and a Leica HCX PL APO 40x/1.10 W CORR objective
272 or a Leica HC PL APO 63x/1.47NA OIL CORR TIRF objective mounted on a Leica DMi8
273 inverted microscope equipped with a live-cell environmental chamber (Okolab) at humidified
274 37°C and 5% CO_2. Imaging mode was Confocal 25 μm. Hoechst images were acquired with a
275 200 mW solid state 405 nm laser and 450/50 nm BP emission filter. Clover images were
276 acquired with a 150 mW solid state 488 nm laser and 525/50 nm BP emission filter. mRuby2
277 images were acquired with a 150 mW solid state 561 nm laser and 620/60 nm BP emission filter.
278 iRFP670 images were acquired with a 140 mW solid state 637 nm laser and 700/75 nm BP
279 emission filter. Z-series covering the full nucleus was acquired at 0.27 μm step size for 40x
280 objective or 0.13 μm step size for 63x objective. For time-lapse imaging, the Z-series was
281 acquired at 0.32 μm step size for 40x objective or 0.16-0.2 μm step size for 63x objective. Two-
282 color images were acquired every 15 seconds. Three-color images were acquired every 15 or 24
283 seconds. Images are a maximum intensity projection of Z-series. Images were processed in
284 Fusion software using ClearView-GPU deconvolution with the Robust (Iterative) algorithm (pre-
285 sharpening 0, 5 iterations, and de-noising filter size 0.1). Linear adjustments in maximum and
286 minimum levels were applied equally across the entire image to display only nuclear spot
287 signals, and not background nuclear fluorescence. Example images of our image processing
288 pipeline are shown in **Supplementary Fig. 2**.
289
290 ***Image analysis***
291 To measure two targeted genomic loci distance in time-lapse images, Fiji image analysis
292 software was used[34]. Z-series acquired at 0.32 μm step size for 40x objective, and 0.16-0.2 μm

293 step size for 63x objective was used. If the nucleus drifted over time, the Correct 3D Drift plugin
294 was used[35]. For segmenting and tracking spots, the TrackMate plugin was used[36]. Blob
295 diameter was set at 2.0 μm. For each channel, threshold was set to include two spots with the
296 maximum intensity in the 3D volume of the nucleus. Simple LAP Tracker used 2 μm linking
297 max distance, 2 μm gap closing max distance, and 2 gap closing max frame gap. Analysis
298 produced "Spots in track statistics" file which was used to run python script to calculate 3D
299 distances between spots and generate 3D tracks. To determine and correct for potential chromatic
300 aberrations, Invitrogen Tetraspeck 0.1 μm Microspheres (ThermoFisher T7279) were imaged.
301 On the Dragonfly High Speed Confocal Platform 505 (Andor), Z-series were acquired for both
302 the Leica HCX PL APO 40x/1.10 W CORR objective and the Leica HC PL APO 63x/1.47NA
303 OIL CORR TIRF objective. TrackMate was then used to localize the positions of the
304 microspheres. iRFP670 and mRuby2 chromatic aberrations in each X,Y,Z dimension were
305 calculated relative to Clover, and corrected by offsetting the shifts in each X,Y,Z dimension as
306 follows:

Objective	**Fluorescent Channel**	**X (μm)**	**Y (μm)**	**Z (μm)**
40x	iRFP670	-0.035	-0.007	+0.691
40x	mRuby2	-0.053	-0.055	+0.319
63x	iRFP670	-0.001	-0.012	+0.147
63x	mRuby2	-0.018	-0.035	-0.028

307

308 ***DNA-FISH***

309 Cells were cultured on 12 mm circle coverslip on 24-well plates and transfected with Casilio
310 components. At 48 hours, cells were fixed with 4% formaldehyde at room temperature for 10

311 min, briefly washed once with 1x PBS, permeabilized with 0.5% PBST for 20 min followed by
312 1x PBS wash, then dehydrated by a series of 75%, 85% and 100% ethanol for 2 min each. Let
313 dry. FISH probe (Cy5-MUC4: /5Cy5/CTTCCTGTCACCGAC, IDT custom DNA oligo) and
314 DNA hybridization buffer were prewarmed and mixed well, added onto slide, covered with cell-
315 attached coverslip, sealed with rubber cement. The sealed cells and probe were then heated on a
316 heat block at 80 °C for 2 min, incubated in a dark humidified chamber at 37 °C overnight. After
317 hybridization, the cell-attached coverslip was unsealed and washed in sequence with 2x SSC at
318 room temperature for 2 min, 10% formamide/2x SSC for 5 min at 45 °C, 2x SSC at room
319 temperature for 5 min, 0.2x SSC at 45 °C for 10 min twice, then counterstained with DAPI for 5
320 min and mounted with SlowFade™ Diamond Antifade Mountant (Invitrogen) for imaging.
321

322 ***Genome track and Hi-C maps***

323 Genome tracks were visualized by UCSC Genome Browser[37]. Hi-C maps were generated
324 using FAN-C[38].

325

326 **Acknowledgments**

327 We thank the Jackson Laboratory Microscopy Service managed by Qianru Yu for microscope
328 usage, Erick Ratamero (Research IT Applications) for imaging analysis support, Jane Cha (JAX
329 Creative) for graphic design, and Research Program Development for help with manuscript
330 editing. This work is partially supported by internal funds provided by the Jackson Laboratory as
331 well as grants from the National Cancer Institute (P30CA034196), the National Human Genome
332 Research Institute (R01-HG009900), and the National Science Foundation (CCF-1955712).
333

334 **Author contributions**

335 J.J.Z. and A.W.C. conceived the study. P.A.C., J.J.Z, and A.W.C. designed the experiments.
336 P.A.C., M.D., N.J., A.T., J.J.Z., and A.W.C. performed the experiments. P.A.C. and M.D.
337 analyzed the data. P.A.C., A.T., J.J.Z., and A.W.C. wrote the manuscript.

338 **Competing interests**

339 A patent application has been filed on the invention.

340 **Data availability**

341 All data is available in the main text or the supplementary materials. Plasmids will be available
342 on Addgene. Raw images will be deposited on open repository.

343 **Code availability**

344 Not applicable.

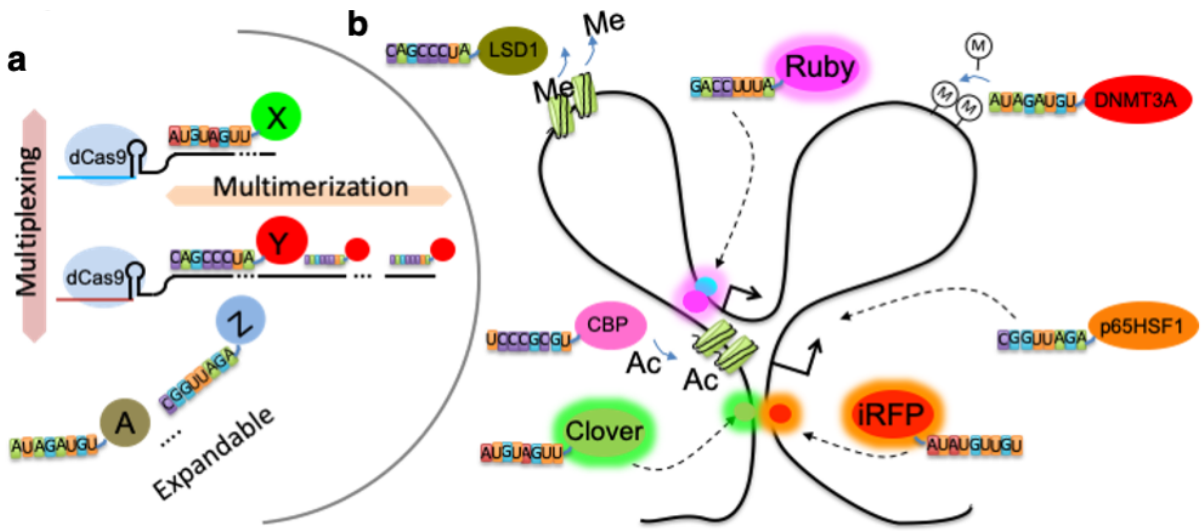

345

346 **Fig. 1. Schematic of Casilio. (a)** Casilio extends CRISPR gRNA with binding sites for Pumilio
347 RNA binding protein-tethered effectors to allow multimerization, multiplexing and expansion of
348 functionalities. **(b)** The potential for Casilio to achieve multimodal operations simultaneously,
349 for example, demethylating histone (using LSD1 module), acetylating histone (CBP),
350 methylating DNA (DNMT3A), activating (p65HSF1) different targets, and at the same time
351 monitoring the localization of multiple locations in live cells.

352

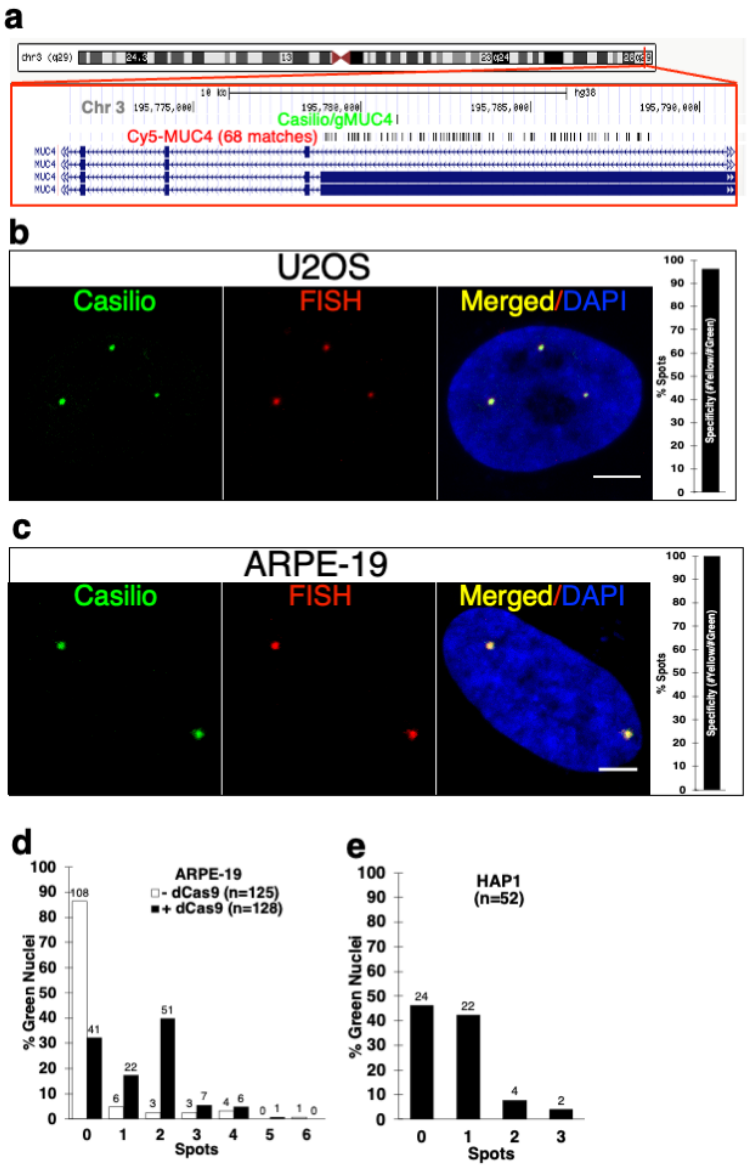

353

354 **Fig. 2. Validation of Casilio imaging specificity. (a)** Schematic showing locations of Casilio

355 MUC4 gRNA (gMUC4) and Cy5-MUC4 FISH probes. **(b)** Co-labeling of *MUC4* locus by

356 Casilio (Green) and DNA-FISH (Cy5-MUC4, Red) in U2OS cells (n=8 nuclei; 28 spots;

357 Specificity=#Red-Green-overlap/#Green=96%). Scale bar, 5 µm **(c)** Co-labeling of Casilio

358 (Green) and DNA-FISH (Cy5-MUC4, Red) in ARPE-19 cells (n=8 nuclei; 16 spots;

359 Specificity=100%). Scale bar, 5 µm **(d)** Percentage of green ARPE-19 nuclei with the indicated

360 numbers of Casilio/gMUC4 spots in live cells without and with dCas9. Counts are indicated on

361 top of the columns. **(e)** Percentage of green HAP1 nuclei with the indicated numbers of

362 Casilio/gMUC4 spots in live cells. Counts are indicated on top of the columns.

363

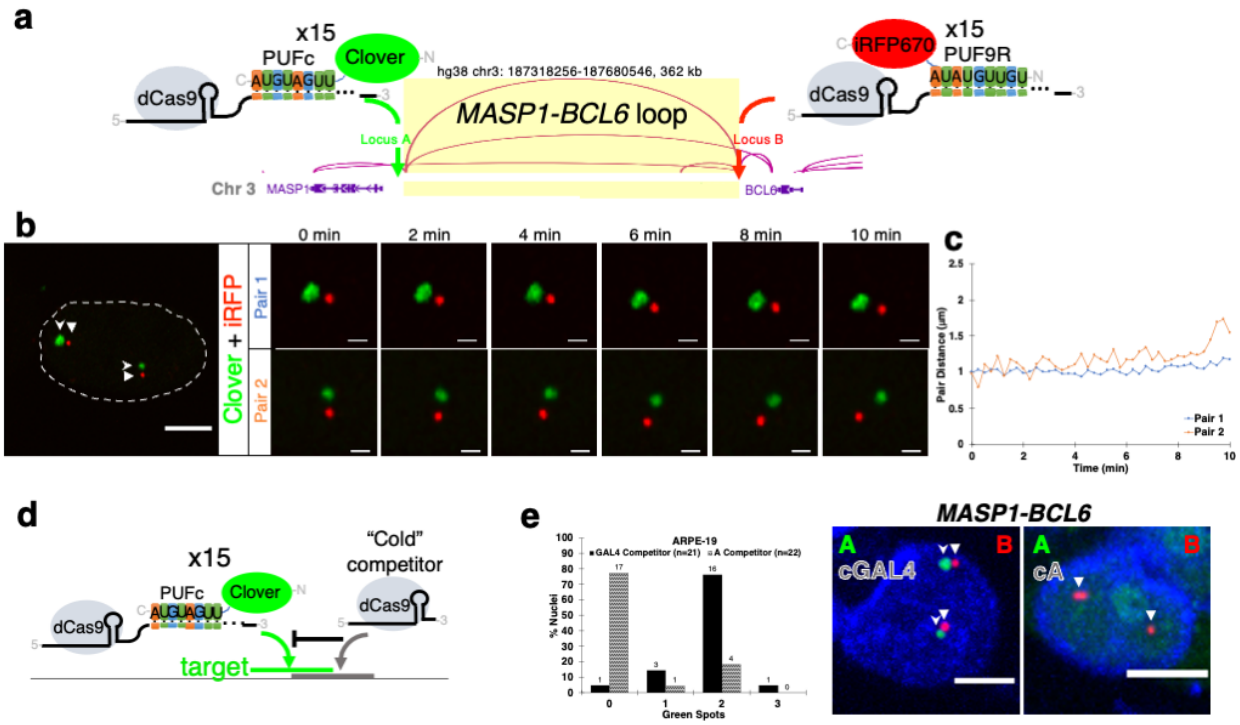

Fig. 3. Casilio live-cell imaging of chromatin interactions and validation. (a) Casilio probes for visualizing chromatin interactions mediated by cohesin, with locus A (5' anchor) labeled by gRNA-15xPBSc/Clover-PUFc and locus B (3' anchor) labeled by gRNA-15xPBS9R/PUF9R-iRFP670. The *MASP1-BCL6* loop with anchors 367 kb apart. **(b)** Representative time-lapse images of the *MASP1-BCL6* loop anchors, locus A near *MASP1* (Clover, green, stealth arrowhead) and locus B near *BCL6* (iRFP670, red, triangle arrowhead), in ARPE-19 cells. Time-lapse image strips show two allelic Pair 1 and Pair 2 at the indicated time points. The whole nucleus at time zero is shown on the left. See Supplementary Video 1. **(c)** Pairwise 3D distances of fluorescent foci in (b) over time. See Supplementary Fig. 1 for all distance plots of imaged nuclei (n=20 nuclei; 33 pairs). **(d)** Schematic of competitor experiment. A "cold" competitor gRNA without Pumilio binding sites (PBS) for fluorescent protein recruitment binds to sequence overlapping a test target. **(e)** Competitor experiments for validating *MASP1-BCL6*. Column plot shows percentages of nuclei with the indicated numbers of Clover (green) spots (counts shown

378 on top of columns) in ARPE-19 cells co-transfected with Clover-PUFc/A-15xPBSc, PUF9R-
379 iRFP670/B-15xBPS9R and either a non-competing GAL4 gRNA (black columns) or a gRNA
380 competing with the corresponding A locus of the loop (patterned columns). Representative
381 images in the non-competed or locus A-competed samples (Clover, green spots and stealth
382 arrowheads; iRFP, red spots and triangle arrowheads) are shown to the right. Whole nucleus
383 scale bars, 5 μm. Time-lapse scale bars, 1 μm.
384

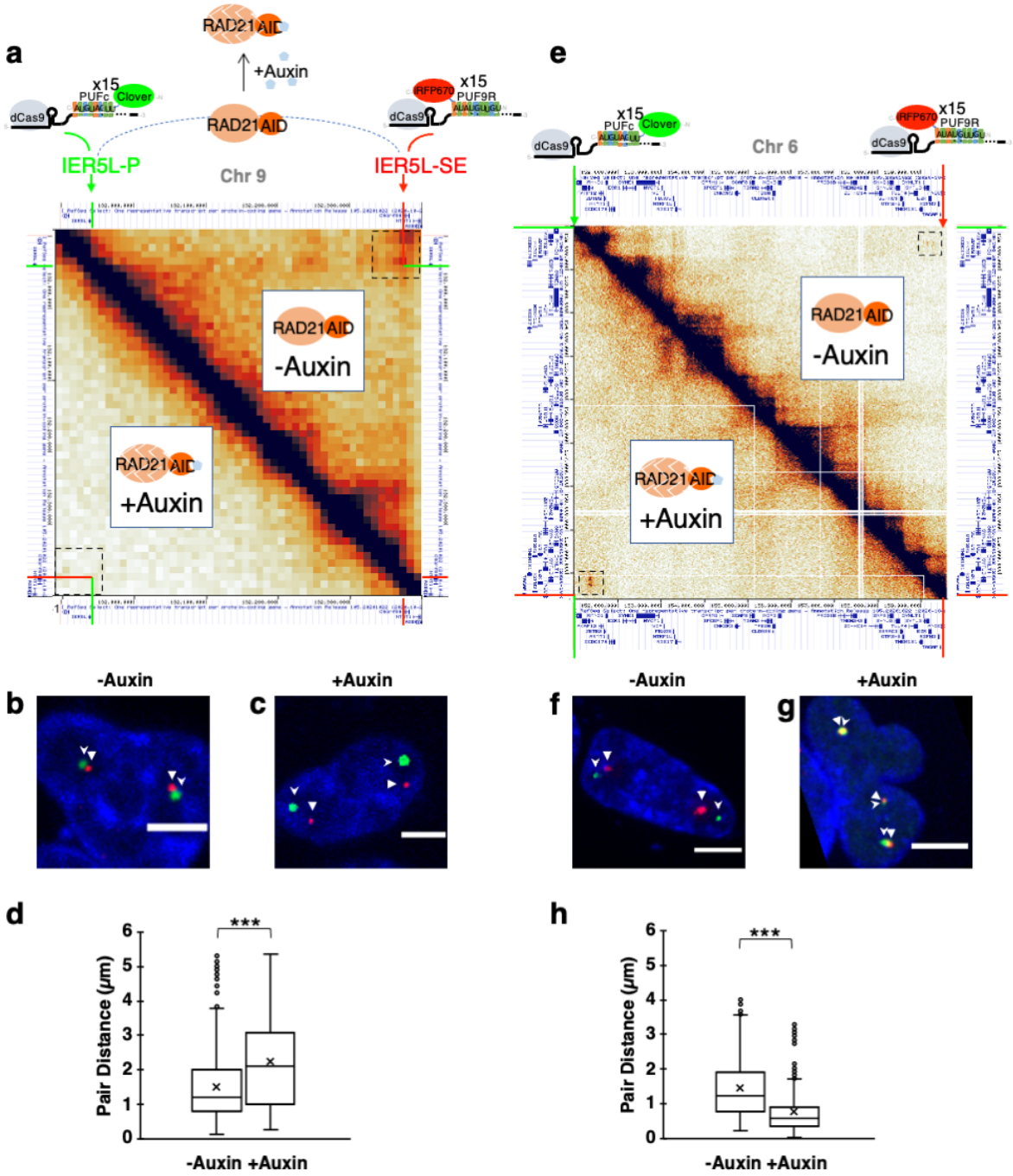

Fig. 4. Casilio visualization of RAD21-dependent and -independent interactions in the presence and absence of RAD21. (a) Schematic of Casilio imaging of chromatin interactions between *IER5L* promoter (*IER5L*-P) and a super enhancer (*IER5L*-SE) in HCT116/RAD21-mAID cells. Hi-C map shows interactions in this region in HCT116/RAD21-mAID cells derived

390 from a previous study[27]. Upper right off-diagonal and lower left off-diagonal plots pairwise
391 interaction between genomic bins in untreated and auxin-treated cells, respectively. Dotted
392 squares mark the area of interest. **(b,c)** Representative images of *IER5L*-P and *IER5L*-SE labeled
393 by Clover (green, stealth arrowhead), and iRFP670 (red, triangle arrowhead), respectively, in
394 nuclei of HCT116/RAD21-mAID cells without (b, see Supplementary Video 2) or with auxin
395 treatment (c, see Supplementary Video 3). Scale bars, 5 μm. (**d)** Boxplot of pairwise spot
396 distances in untreated (n=1325 measurements of 33 pairs from 18 nuclei; mean=1.52 μm, x-
397 marked; median=1.21 μm, line inside box) and auxin-treated (n=1435 measurements of 35 pairs
398 from 20 nuclei; mean= 2.26 μm; median=2.09 μm) cells. ***Mann-Whitney test two-sided
399 $p<0.00001$. **(e)** Hi-C map showing the pairwise interaction between genomic bins encompassing
400 a RAD21-independent loop in untreated (upper right off-diagonal) and auxin-treated (lower left
401 off-diagonal) cells. Dotted squares mark the area of interest. **(f,g)** Representative images of the
402 RAD21-independent interaction labeled by Clover (green, stealth arrowhead), and iRFP670 (red,
403 triangle arrowhead), respectively, in nuclei of HCT116/RAD21-mAID cells without (f, see
404 Supplementary Video 4) or with auxin treatment (g, see Supplementary Video 5). Scale bars, 5
405 μm. (**h)** Boxplot of pairwise spot distances in untreated (n=1046 measurements of 27 pairs from
406 18 nuclei; mean=1.44 μm, x-marked; median=1.24 μm, line inside box) and auxin-treated
407 (n=921 measurements of 25 pairs from 20 nuclei; mean= 0.76 μm; median= 0.57 μm) cells.
408 ***Mann-Whitney test two-sided $p<0.00001$.

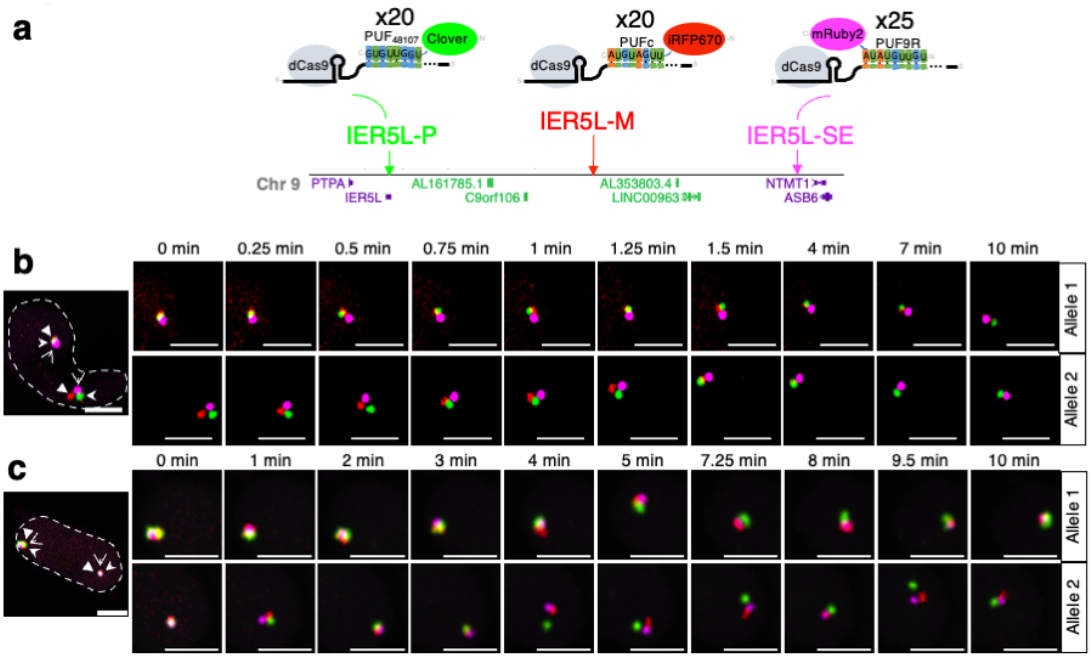

Fig. 5. Three-color three-point live-cell imaging of chromatin loops. (a) Casilio probes for visualizing chromatin interactions of *IER5L* promoter and its super-enhancer, with locus P (promoter) labeled by gRNA-20xPBS$_{48107}$/Clover-PUF$_{48107}$, locus M (mid-point) labeled by gRNA-20xPBSc/iRFP670-PUFc, and locus SE (super-enhancer) labeled by gRNA-25xPBS9R/PUF9R-mRuby2. **(b,c)** Representative nuclei (nuclear boundaries outlined) and time-lapse images of *IER5L*-P-SE loop, with *IER5L* promoter, midpoint and super-enhancer labeled by Clover (green, stealth arrowhead), iRFP670 (red, triangle arrowhead), mRuby2 (magenta, open arrowhead), respectively, in HCT116 cells at the indicated time point. Scale bars 5 µm. See Supplementary Videos 6 and 7. See Supplementary Fig. 6 for distance plots of imaged nuclei (n=18 nuclei; 28 alleles).

References

1. Maass, P.G., A.R. Barutcu, and J.L. Rinn, *Interchromosomal interactions: A genomic love story of kissing chromosomes.* J Cell Biol, 2019. **218**(1): p. 27-38.
2. Mishra, A. and R.D. Hawkins, *Three-dimensional genome architecture and emerging technologies: looping in disease.* Genome Med, 2017. **9**(1): p. 87.
3. Krumm, A. and Z. Duan, *Understanding the 3D genome: Emerging impacts on human disease.* Semin Cell Dev Biol, 2019. **90**: p. 62-77.
4. Fullwood, M.J., et al., *An oestrogen-receptor-alpha-bound human chromatin interactome.* Nature, 2009. **462**(7269): p. 58-64.
5. Lieberman-Aiden, E., et al., *Comprehensive mapping of long-range interactions reveals folding principles of the human genome.* Science, 2009. **326**(5950): p. 289-93.
6. Lakadamyali, M. and M.P. Cosma, *Visualizing the genome in high resolution challenges our textbook understanding.* Nature Methods, 2020.
7. Robinett, C.C., et al., *In vivo localization of DNA sequences and visualization of large-scale chromatin organization using lac operator/repressor recognition.* J Cell Biol, 1996. **135**(6 Pt 2): p. 1685-700.
8. Alexander, J.M., et al., *Live-cell imaging reveals enhancer-dependent Sox2 transcription in the absence of enhancer proximity.* Elife, 2019. **8**.
9. Lindhout, B.I., et al., *Live cell imaging of repetitive DNA sequences via GFP-tagged polydactyl zinc finger proteins.* Nucleic Acids Res, 2007. **35**(16): p. e107.
10. Casas-Delucchi, C.S., et al., *Targeted manipulation of heterochromatin rescues MeCP2 Rett mutants and re-establishes higher order chromatin organization.* Nucleic Acids Res, 2012. **40**(22): p. e176.
11. Ma, H., P. Reyes-Gutierrez, and T. Pederson, *Visualization of repetitive DNA sequences in human chromosomes with transcription activator-like effectors.* Proc Natl Acad Sci U S A, 2013. **110**(52): p. 21048-53.
12. Ren, R., et al., *Visualization of aging-associated chromatin alterations with an engineered TALE system.* Cell Res, 2017. **27**(4): p. 483-504.
13. Sander, J.D. and J.K. Joung, *CRISPR-Cas systems for editing, regulating and targeting genomes.* Nat Biotechnol, 2014. **32**(4): p. 347-55.
14. Chen, B., et al., *Dynamic imaging of genomic loci in living human cells by an optimized CRISPR/Cas system.* Cell, 2013. **155**(7): p. 1479-91.
15. Tanenbaum, M.E., et al., *A protein-tagging system for signal amplification in gene expression and fluorescence imaging.* Cell, 2014. **159**(3): p. 635-46.
16. Ma, H., et al., *Multiplexed labeling of genomic loci with dCas9 and engineered sgRNAs using CRISPRainbow.* Nat Biotechnol, 2016. **34**(5): p. 528-30.
17. Qin, P., et al., *Live cell imaging of low- and non-repetitive chromosome loci using CRISPR-Cas9.* Nat Commun, 2017. **8**: p. 14725.
18. Ma, H., et al., *CRISPR-Sirius: RNA scaffolds for signal amplification in genome imaging.* Nat Methods, 2018. **15**(11): p. 928-931.
19. Maass, P.G., et al., *Spatiotemporal allele organization by allele-specific CRISPR live-cell imaging (SNP-CLING).* Nat Struct Mol Biol, 2018. **25**(2): p. 176-184.
20. Wang, H., et al., *CRISPR-mediated live imaging of genome editing and transcription.* Science, 2019. **365**(6459): p. 1301-1305.

21. Cheng, A.W., et al., *Casilio: a versatile CRISPR-Cas9-Pumilio hybrid for gene regulation and genomic labeling.* Cell Res, 2016. **26**(2): p. 254-7.
22. Chen, Y. and G. Varani, *Engineering RNA-binding proteins for biology.* Febs j, 2013. **280**(16): p. 3734-54.
23. Wang, Y., et al., *Engineering splicing factors with designed specificities.* Nat Methods, 2009. **6**(11): p. 825-30.
24. Taghbalout, A., et al., *Enhanced CRISPR-based DNA demethylation by Casilio-ME-mediated RNA-guided coupling of methylcytosine oxidation and DNA repair pathways.* Nat Commun, 2019. **10**(1): p. 4296.
25. Gilbert, L.A., et al., *CRISPR-mediated modular RNA-guided regulation of transcription in eukaryotes.* Cell, 2013. **154**(2): p. 442-51.
26. Natsume, T., et al., *Rapid Protein Depletion in Human Cells by Auxin-Inducible Degron Tagging with Short Homology Donors.* Cell Rep, 2016. **15**(1): p. 210-218.
27. Rao, S.S.P., et al., *Cohesin Loss Eliminates All Loop Domains.* Cell, 2017. **171**(2): p. 305-320.e24.
28. Li, G., et al., *ChIA-PET2: a versatile and flexible pipeline for ChIA-PET data analysis.* Nucleic Acids Res, 2017. **45**(1): p. e4.
29. Zhu, J.J. and A.W. Cheng, *JACKIE: Fast enumeration of single- and multi-copy CRISPR binding sites.* bioRxiv, 2020: p. 2020.02.27.968933.
30. Bae, S., J. Park, and J.S. Kim, *Cas-OFFinder: a fast and versatile algorithm that searches for potential off-target sites of Cas9 RNA-guided endonucleases.* Bioinformatics, 2014. **30**(10): p. 1473-5.
31. Shcherbakova, D.M. and V.V. Verkhusha, *Near-infrared fluorescent proteins for multicolor in vivo imaging.* Nat Methods, 2013. **10**(8): p. 751-4.
32. Lam, A.J., et al., *Improving FRET dynamic range with bright green and red fluorescent proteins.* Nat Methods, 2012. **9**(10): p. 1005-12.
33. Cong, L., et al., *Multiplex genome engineering using CRISPR/Cas systems.* Science, 2013. **339**(6121): p. 819-23.
34. Schindelin, J., et al., *Fiji: an open-source platform for biological-image analysis.* Nat Methods, 2012. **9**(7): p. 676-82.
35. Parslow, A., A. Cardona, and R.J. Bryson-Richardson, *Sample drift correction following 4D confocal time-lapse imaging.* J Vis Exp, 2014(86).
36. Tinevez, J.Y., et al., *TrackMate: An open and extensible platform for single-particle tracking.* Methods, 2017. **115**: p. 80-90.
37. Kent, W.J., et al., *The human genome browser at UCSC.* Genome Res, 2002. **12**(6): p. 996-1006.
38. Kruse, K., C.B. Hug, and J.M. Vaquerizas, *FAN-C: a feature-rich framework for the analysis and visualisation of chromosome conformation capture data.* Genome Biol, 2020. **21**(1): p. 303.